Oxygen Reduction Reaction in Alkaline Media Causes Iron Leaching from Fe–N–C Electrocatalysts

Yu-Ping Ku, Konrad Ehelebe, Andreas Hutzler, Markus Bierling, Thomas Böhm, Andrea Zitolo, Mykhailo Vorokhta, Nicolas Bibent, Florian Speck, Dominik Seeberger, et al.

Oxygen Reduction Reaction in Alkaline Media Causes Iron Leaching from Fe-N-C Electrocatalysts

Yu-Ping Ku[a,b,*], Konrad Ehelebe[a,b], Andreas Hutzler[a], Markus Bierling[a,b], Thomas Böhm[a], Andrea Zitolo[c], Mykhailo Vorokhta[d], Nicolas Bibent[e], Florian D. Speck[a,b], Dominik Seeberger[a,b], Ivan Khalakhan[d], Karl J. J. Mayrhofer[a,b], Simon Thiele[a,b], Frédéric Jaouen[e,*], Serhiy Cherevko[a,*]

[a] Forschungszentrum Jülich GmbH, Helmholtz-Institute Erlangen-Nürnberg for Renewable Energy (IEK-11), Cauerstraße 1, 91058 Erlangen, Germany

[b] Department of Chemical and Biological Engineering, Friedrich-Alexander University Erlangen-Nürnberg, Cauerstraße 1, 91058 Erlangen, Germany

[c] Synchrotron SOLEIL, L'orme des Merisiers, BP 48 Saint Aubin, 91192 Gif-sur-Yvette, France

[d] Charles University, Faculty of Mathematics and Physics, Department of Surface and Plasma Science, V Holešovičkách 2, 18000 Prague 8, Czech Republic

[e] Institut Charles Gerhardt Montpellier, Univ. Montpellier, CNRS, ENSCM, 1919 route de Mende, F-34293 Montpellier, France

KEYWORDS: Fe-N-C, Oxygen Reduction Reaction, AEMFC, Fe dissolution, Fe redox transition

ABSTRACT: The electrochemical activity of modern Fe-N-C electrocatalysts in alkaline media is on par with that of platinum. For successful application in fuel cells, however, also high durability and longevity must be demonstrated. Currently, a limited understanding of degradation pathways, especially under operando conditions, hinders the design and synthesis of simultaneously active and stable Fe-N-C electrocatalysts. In this work, using a gas diffusion electrode half-cell coupled with inductively coupled plasma mass spectrometry setup, Fe dissolution is studied under conditions close to those in fuel cells, i.e. with porous catalyst layer and at current densities up to -125 mA·cm^{-2}. Varying the rate of oxygen reduction reaction, we show a remarkable linear correlation between the Faradaic charge passed through the electrode and the amount of Fe dissolved from the electrode. This finding is rationalized assuming that oxygen reduction and Fe dissolution reactions are interlinked, likely through a common intermediate formed during the Fe redox transitions in Fe species involved in oxygen reduction reaction, such as FeN_xC_y and Fe_3C@N-C. Moreover, such a linear correlation allows the application of a simple metric – S-number – to report the material's stability. Hence, in the current work, a powerful tool for a more applied stability screening of different electrocatalysts is introduced, which allows on the one hand fast performance investigations under more realistic conditions, and on the other hand more advanced mechanistic understanding of Fe-N-C degradation in catalyst layers.

1. Introduction

On the way to a climate neutral *hydrogen economy*,[1] energy efficient, durable and affordable fuel cells (FCs) are needed. While proton exchange membrane fuel cells (PEMFCs) have been commercialized, further development of this technology is hindered by its dependency on Pt as the main electrocatalyst material for both hydrogen oxidation reaction (HOR) and oxygen reduction reaction (ORR).[2] Therefore, research on highly active and stable platinum group metal (PGM)-free catalysts is booming, as summarized in recent reviews.[3] Among all identified PGM-free candidates, iron-nitrogen-doped carbon (Fe-N-C) is the most promising to catalyze the sluggish ORR.[4, 5] Recent studies have theoretically and experimentally demonstrated that Fe-N-C catalysts are more active and stable in alkaline than in acidic media.[6-8] This indicates the unique possibility to use Fe-N-C as a relatively efficient, earth abundant and cheap cathode catalyst material in the alternative anion exchange membrane fuel cell (AEMFCs) technology. Due to the recent groundbreaking developments in membrane science, AEMFCs demonstrate great potential for

successful commercialization.[9] With regards to durability and longevity of Fe-N-C catalysts in this environment, many questions remain however open. In particular, understanding of Fe^{x+} leaching and, consequently, an implementation of mitigation strategies to its suppression are considered main challenges.[4, 6, 10-12]

So far, four key degradation mechanisms have been suggested to occur in parallel or series on Fe-N-C in acidic media,[5] providing also clues to possible degradation pathways in alkaline electrolytes:

(i) *Carbon corrosion*. Corrosion of the carbon support leads to Fe demetallation and a drop in electron conductivity.[5, 10] It has been shown in various studies that the rate of this mechanism depends on temperature,[10] electrochemical potential,[10, 13] and, as was demonstrated recently, on the presence or absence of O_2 in aqueous electrolytes.[14]

(ii) *Reactive oxygen species (ROS).* Formed as intermediates or by-products of ORR, ROS were shown to cause Fe-N-C catalyst degradation in acidic conditions.[8, 14-16] ROS can oxidize the carbon support surface, resulting in a decrease of the ORR turnover frequency (TOF) of the existing Fe active sites. The presence, amount and effect of ROS depend on the electrochemical potential, temperature, and presence of ORR.[8, 16] In an alkaline environment the effect of ROS attack on catalyst degradation was shown to be minor.[8, 16]

(iii) *Agglomeration.* Agglomeration of active single-atom Fe sites to Fe-clusters was shown to be affected by temperature.[17]

(iv) *Fe dissolution.* Direct Fe ion leaching from active sites (not indirectly triggered by carbon corrosion) is influenced by electrolyte pH,[6] potential,[10] temperature,[10] chemical environment,[6] and water-flux across the active sites within micropores.[13]

While it is likely that several degradation mechanisms are operative and the extent of each mechanism is different depending on the FC operating conditions, the Fe-N-C structure and morphology, and the active layer design, a fundamental understanding of the stability of Fe-N-C catalysts is still lacking. The dissolution of different Fe-containing species initially present in Fe-N-C catalysts could lead to various types and degrees of degradation.[12] For instance, Fe leaching from atomically dispersed FeN_xC_y sites, which catalyze ORR in both acidic and alkaline media, will result in a decreasing active site density (SD). The turnover frequency (TOF) of active sites may also be modified. For example, Fe_3C particles embedded within graphite (Fe_3C@N-C) could act as an electron-donor to nearby FeN_xC_y sites[18] and/or graphite layers.[19] As a result, the adsorption of O_2 can be optimized, and the TOF of active sites can be increased, especially in alkaline media.[20] Therefore, Fe leaching from Fe_3C@N-C in alkaline media might cause a drop of TOF of originally boosted active sites. Furthermore, Fe leaching from different Fe species was observed during stability tests under various conditions.[10, 11, 13, 21] As an example, in scanning flow cell (SFC) experiments coupled to inductively coupled plasma mass spectroscopy (ICP-MS), Fe dissolution in an Ar-purged acidic electrolyte was assigned to leaching of inactive Fe sites.[10, 11] In contrast, for cathodes after H_2/O_2 PEMFC tests, the decrease of ORR activity was correlated to a loss of FeN_xC_y active sites using *ex situ* Mössbauer spectroscopy.[13, 21] This discrepancy illustrates that direct comparisons of the results from thin-film catalyst layers in aqueous model systems (AMS), e.g. rotating disk electrode (RDE) or SFC, and gas-diffusion cathodes in PEMFCs or AEMFCs are challenging, as highlighted in our recent review.[22] Such differences may affect the intensity and the mechanisms of degradation significantly. A major discrepancy between AMS and real devices is the direct contact of the catalyst to gaseous O_2, which cannot be realized in RDE or SFC. Moreover, even in AMS, the influence of O_2 on Fe-N-C stability is rarely addressed as the stability has traditionally been tested in de-aerated acidic environment. However, degradation of PGM-free materials can be significantly affected by the presence of O_2.[14, 23, 24] Thus, using online ICP-MS, Speck *et al*.[23] identified different dissolution mechanisms for MnO_x in Ar- and O_2-purged alkaline media. On the one hand, Mn transient-dissolution occurs in both Ar and O_2 environment, which was attributed to the redox transitions of Mn. On the other hand, Mn total dissolution is drastically increased in O_2 environment. This was ascribed to the presence of ROS, such as HO_2^- generated during the ORR. A similar trend has also been detected for Fe-N-C catalysts degradation in acidic media. Combining RDE measurements with Raman spectroscopy, Kumar *et al*.[14] showed that both deterioration of ORR activity and the extent of carbon corrosion are significantly more severe in O_2- compared to Ar-saturated electrolytes.

In order to bridge the gap between fundamental and applied research, gas diffusion electrode (GDE) half-cell setups have emerged as a tool to combine the advantages of AMS (three electrode setup, fast and comparable testing at standard operating conditions) and FCs (aqueous electrolyte-free catalyst layers and high current densities).[25, 26-28] In the present work, we used a GDE half-cell setup coupled with online ICP-MS (GDE-ICP-MS)[29] to systematically investigate the impact of O_2 atmosphere and a solid electrolyte interface on Fe demetallation in alkaline medium from Fe-N-C catalyst layers (CLs) operating at current densities up to -125 $mA \cdot cm^{-2}$. Such a setup allows going beyond the previously reported SFC-ICP-MS setup, which was restricted to very low current densities and therefore of little interest to study degradation mechanisms that are intimately related to the ORR rate.

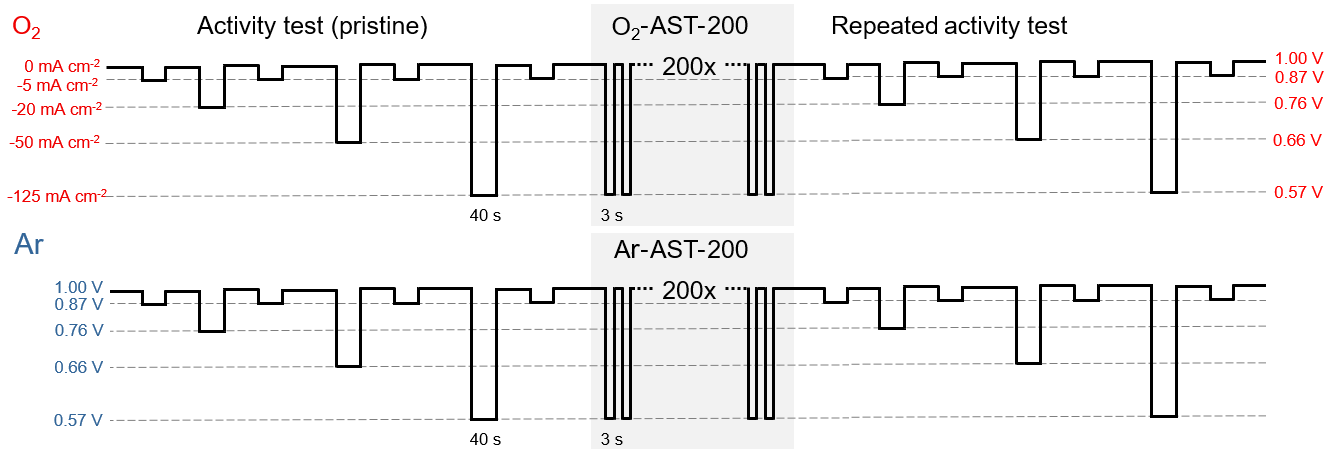

Scheme 1. Electrochemical protocols of the GDE-ICP-MS measurements in O_2 and Ar environments, respectively. The protocol with O_2 consists of an initial activity test, an AST of 200 cycles and a final activity test. The applied current densities are shown on the left hand-side of the upper scheme and the measured steady-state potential responses are shown on the right hand-side. This set of potentials is then applied in the protocol with Ar, shown in the lower scheme.

2. Experimental

2.1 Electrode manufacturing

There are two kinds of alkaline Fe-N-C gas diffusion electrodes (GDEs) in this work. One contains a commercial Fe-N-C catalyst (PMF-011904,[30] Lot 0601, Pajarito Powder) and the other contains a benchmark synthesized Fe-N-C catalyst ($Fe_{0.5}$-NH_3). A brief description of the manufacture of the electrode containing PMF-011904 can be found below, and a detailed version is in section 1.1.1 of the supporting information (SI). The synthesis of $Fe_{0.5}$-NH_3 and the manufacture of its electrode can be found in sections 1.1.2 and 1.1.3 of the SI, respectively. Note that in the Results and Discussion sections 3.1 and 3.2, the Fe-N-C catalyst refers to PMF-011904, while in the section 3.3 both Fe-N-C catalysts are considered and specified accordingly.

The alkaline Fe-N-C catalyst layer (CL) was fabricated on a gas diffusion medium including a microporous layer (H23C8, Freudenberg, 4x4 cm^2, 218 ± 5 µm). The CL with PMF-011904 was composed of 70 ± 0.3 wt% the commercial Fe-N-C catalyst and 30 ∓ 0.3 wt% commercial ionomer (Aemion™ HNN5-00-X, Ionomr). The anion exchange membrane (AEM) was prepared solely with this ionomer. The loading of the CL was determined to be 1.35 ± 0.05 $mg{\cdot}cm^{-2}$. The thicknesses of the CL and AEM are 47.5 ± 5.2 µm and 0.5 ± 0.2 µm, respectively, measured from images (see Figure S2 and Table S2) taken via cross-sectional imaging with a focused ion beam scanning electron microscope (Crossbeam 540 FIB-SEM, Zeiss). More detailed information can be found in section 1.2 of the SI.

2.2 GDE-ICP-MS measurements

Both on-line GDE-ICP-MS and *ex situ* ICP-MS measurements were performed. The GDE-ICP-MS setup and methodology have been introduced in our previous work.[29] Also, Scheme S1 demonstrates the concept of the setup. To detect ^{56}Fe species, ICP-MS (Perkin Elmer, NexION 350) was operated in dynamic reaction cell (DRC) mode using CH_4 (5.5, Air Liquide) to minimize the impact of the interference with $^{40}Ar^{16}O^+$. An internal standard of 100 $\mu g{\cdot}L^{-1}$ of Ge ($(NH_4)_2GeF_6$, Merck Centripur) in 1 wt% HNO_3 (Suprapur®, Merck) was used. A four-point calibration was carried out with a blank and three standard Fe solutions (0, 1, 5, 25 $\mu g_{Fe}{\cdot}L^{-1}$) every day before measurements. For the standard solutions, the Merck Centripur ICP standard ($Fe(NO_3)_3$, 1000 $mg{\cdot}L^{-1}$, in 2–3% HNO_3) was first diluted 100 times with 1 wt% $HNO_{3(aq)}$, and then further diluted to the aimed concentrations with a 0.1 M NaOH electrolyte (Merck Suprapure). More details can be found in section 1.3 of the SI.

The electrochemical measurements were performed in 0.1 M NaOH in a GDE half-cell.[27, 28] With GDE-ICP-MS, the impact of (i) gas supplied to the back of the GDE (Ar vs. O_2, 50 $ml{\cdot}min^{-1}$) and (ii) the CL | electrolyte interface (AEM vs. no AEM) have been investigated. The measurements with O_2 were conducted with galvanostatic techniques and consisted of three parts, (i) an activity test, (ii) an accelerated stress test of 200 cycles (AST-200), and finally (iii) a repeated activity test. (see Scheme 1). Then, with the potential responses obtained from the first activity test with O_2, an electrochemical protocol with Ar-saturated environment was programed with potentiostatic techniques that reproduced the potentials experienced by the GDEs during the whole measurements with O_2 (also see Scheme 1). Importantly, this protocol with Ar was applied to fresh samples, not to samples after the O2 protocol. After the whole Ar protocol, the activity test with O_2 was performed. A detailed explanation of this experimental design can be found in section 1.4 of the SI. Each set of experiments was performed at least twice to show the result's reproducibility.

To obtain long-term dissolution stability data, the respective ASTs in Ar and O_2 protocols were also extended from 200 to 2000 cycles, noted as AST-Ar-2k and AST-O_2-2k, respectively. Every 500 cycles, two aliquots of solution were taken out from the well-mixed electrolyte for *ex situ* ICP-MS measurements. Following these extended ASTs, a final ORR activity test was also performed.

All values of potential are reported with respect to a reversible hydrogen electrode (RHE) and 100 % iR-corrected. The reference electrode (RE, Ag/AgCl Metrohm) was calibrated every day ($E_{Ag/AgCl} = 0.944 \pm 0.0115\ V_{RHE}$). For potentiostatic measurements (Ar environment), the potential was 80 % iR-compensated during measurements and 20 % iR-corrected post measurements. The uncompensated resistance (R_u) was determined via electrochemical impedance spectroscopy (EIS) at open circuit potential (OCP). For galvanostatic measurements (O_2), the data was 100 % post iR-corrected. The R_u was measured via EIS at each current step, as proposed previously.[26, 27] In all experiments, the electrolyte was always purged with 50 ml·min^{-1} Ar.

Experimental details on characterization of catalysts and catalyst layers can be found in sections 1.5 - 1.8 of the SI.

3. Results and Discussion

3.1 Online Fe Dissolution in Varied Conditions and the Respective Impacts on ORR performance

In order to gain insights into the Fe-N-C demetallation in realistic alkaline CLs during ORR, Fe dissolution in Ar- and O_2-environments is first compared during the application of similar potential steps. Figure 1 shows the effect of O_2 (or ORR) on the Fe dissolution at different potentials between 0.57 and 0.87 V_{RHE}. The novel GDE-ICP-MS setup allows detection of Fe dissolution at current densities up to -125 mA·cm^{-2} (see Figure 1A). The highest current density that can be reached with this setup is defined by the electrolyte resistance, which is in turn mainly limited by the highest alkaline electrolyte concentration that the ICP-MS can tolerate, i.e. 0.1 M. For comparison: in AMS such as RDE, only a few mA·cm^{-2} can be reached due to the solubility limit of O_2 in aqueous electrolytes.[10, 14, 31]

In Figure 1A and 1B, the electrochemical protocols in Ar and O_2 environments before their respective AST-200 protocols are displayed. In the presence of O_2, -125 mA·cm^{-2} can be reached due to ORR at around 0.6 V_{RHE}. In an Ar environment the steady-state current density, which was not yet reached at the end of the 40-s step, is less negative than -0.2 mA·cm^{-2} at similar potentials. Under these electrochemical conditions, the Fe dissolution profiles (see Figure 1C, left hand-side axis, solid lines) show that significantly more Fe is dissolved in the presence of O_2. In the potential range between 0.8 – 0.6 V_{RHE}, the amount of Fe dissolved during each 40-s step in O_2 is about one order of magnitude higher than that in Ar (see Figure 1C, right hand-side axis, dotted lines). Also, at 0.87 V_{RHE}, the Fe dissolution is already significantly higher in O_2 than in Ar. Hence, it is clear that the amount of Fe dissolution would be underestimated if the electrochemical testing is executed in an environment without O_2 as often done hitherto in AMS.[6, 10]

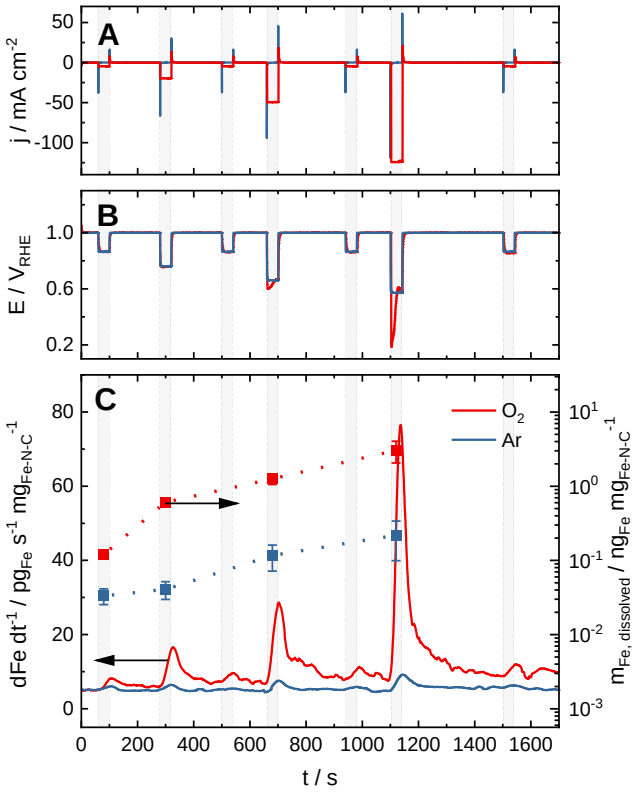

Figure 1. Comparison of Fe-N-C demetallation between Ar- and O_2-saturated alkaline (0.1 M NaOH) environments before the accelerated stress test (AST-200), via gas diffusion electrode setup coupled to inductively coupled plasma mass spectrometry (GDE-ICP-MS). A: Current density profile. B: Potential profile. C-left axis (solid lines): Fe dissolution rate normalized to catalyst loading. C-right axis (dotted lines): Amount of dissolved Fe species at different potentials (V_{RHE}) normalized to catalyst loading.

In addition to the impact of the presence of O_2 or ORR, the following two characteristic features of Fe-N-C demetallation can be observed for both Ar and O_2 cases. Firstly, the Fe dissolution starts immediately when the cathodic currents or potential steps are applied. After moving back to open circuit potential (OCP), also the dissolution drops immediately. In general, the amount of dissolved Fe species rises with decreasing potential or/and increasing current density. Additionally, the dissolution rate at the regularly repeated steps performed at -5 mA·cm^{-2} (or at the corresponding potential, 0.87 V) is almost constant (see Figure S3C), indicating that the order of the applied steps at higher currents (or lower potentials) does not affect the dissolution behavior in the chosen protocol. Besides Fe dissolution, also the potential at these repeated steps merely drops 3 mV before the step to the

lowest potential before the accelerated stress test (AST-200) (see Figure S3B).

To mimic fuel cell load cycles, we conducted the 200-cycle AST between -0.05 and -125 mA·cm^{-2} in O_2 environment, which correspond to 0.88 ± 0.03 and 0.56 ± 0.04 V_{RHE}, respectively. For comparison, the AST in Ar was conducted in a similar potential range, i.e. between 1.0 and 0.573 V_{RHE}. Using these protocols, the total amount of dissolved Fe species during the O_2-AST-200 is almost one order of magnitude higher than that during the Ar-AST-200 (see Figure 2A), in line with the trends seen already during the part of the protocol that is applied before the AST-200.

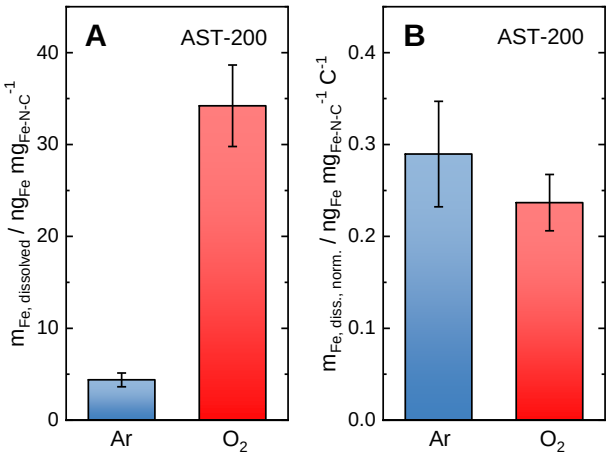

Figure 2. Comparison of the quantitative results for the Fe dissolution in alkaline (0.1 M NaOH) during the AST-200 between Ar- and O_2-saturated environments. A: Amount of dissolved Fe species normalized to catalyst loading. B: Amount of dissolved Fe species normalized to the catalyst loading and normalized also to the applied electric charge (O_2 environment) or measured electric charge (Ar environment).

Interestingly, despite the dramatically higher Fe dissolution during ORR compared to the one in Ar environment, the electric-charge-normalized dissolution rates during the ASTs in O_2 and Ar are similar (see Figure 2B). This implies that Fe dissolution in Fe-N-C could be associated with a charge-transfer-related process that commonly occurs in both ASTs in Ar and O_2. To further validate this linear correlation between total amount of Fe dissolved from and the total electric charge passed through the electrode, Fe dissolution in O_2 for two different holding periods at -125 mA·cm^{-2} (40 s or 600 s) is compared in Figure S4A. The results confirm that Fe dissolution is fairly constant when being normalized to the applied electric charge. In contrast, when the same Fe dissolution data is normalized to the number of applied cycles, no correlation can be seen (see Figure S4B). All these results imply that the rate of Fe dissolution in alkaline media is directly proportional to the applied current density, at least within the corresponding investigated potential range. This finding could partly explain why Sgarbi *et al.*[12] did not observe a notable deviation in Fe-N-C degradation between Ar- and O_2–saturated alkaline environments with an RDE half-cell, where the current density of ORR is limited to around -5 mA/cm^2 or lower. While the fate of leached iron cations can depend on the Fe-N-C catalyst morphology (microporous Fe-N-C in the previous work[12] vs. mesoporous Fe-N-C in the present work, the former possibly favoring reprecipitation in the catalytic layer and the latter favoring the transfer towards the bulk electrolyte), a 25 times higher current density achieved in a GDE half-cell here amplifies the difference and unveils the impacts of ORR on Fe-N-C degradation in alkaline media, of which a detailed evaluation can be found in the section 3.3.

In oxygen evolution reaction (OER) research, the reciprocal of the charge-normalized dissolution, the so-called S-number, has been well established as a metric for catalyst stability.[32] Due to the correlation between electric charge and Fe dissolution, a similar concept can be applied here. The S-number of the presently studied commercial Fe-N-C would be around 10^6. This means that in the studied potential region between 0.57 and 0.87 V_{RHE}, about one million electrons were exchanged in the ORR for every Fe atom that dissolved. Accordingly, the average probability of losing an Fe atom for each electron transfer event is approximately 10^{-6}. Yet, as the degradation rate of Fe-N-C catalysts might depend on operation time, as shown for acidic ORR,[33] so would be their S-numbers. Hence, we additionally performed *ex situ* experiments with the respective ASTs extended from 200 to 2000 cycles, noted as Ar-AST-2k and O_2-AST-2k. Especially, the S-numbers obtained during O_2-AST-2k and evaluated for every 500 cycles (see Figure S5) suggest that the S-number around 10^6 is representative for the first 1500 cycles. Further discussion on how applicable this S-number is for AEMFCs can be found in the text accompanying Figure S5. Although ORR is a complicated multi-step 4-electron-transfer reaction with several intermediate states,[34, 35] where the coordinated Fe cation could be variously unstable, the S-number could be a suitable quantification metric to study the overall stability of Fe-N-C catalysts in various conditions and to compare different materials.

To further approach more realistic AEMFC conditions, we additionally compare on-line Fe dissolution in GDEs without and with a thin AEM coated on top of the CL in an O_2-saturated environment. For Pt/C catalysts in acidic media, a significant stabilizing impact of Nafion membranes on the net Pt dissolution was recently observed.[29] This effect was attributed to the impeded mass-transport of dissolved catalyst species through the membrane. However, for the present system, we cannot observe any significant impact of the AEM on Fe dissolution (see Figure 3C and S6). The diverging effects of the Nafion membranes and the AEM can be attributed to the following differences between the two systems. Firstly, the thickness ratio of CL to membrane in our AEM system is two to three orders of magnitude higher than that in the work mentioned above (see Table S2 and Figure S2). In our

case, the doctor-blade coated AEM membrane is less than 1 µm thick, whereas in the literature Nafion membranes of 25 and 52 µm were used.[29] Hence, the impacts of AEM on Fe-N-C demetallation in our study are diminished. Additionally, the varied physical properties of dissolved species and the membranes could contribute to the differing results.[5] For future work, commercial AEMs with increased thickness should be used to reveal the impact of the transport of dissolved Fe species through the membrane on the total Fe dissolution.

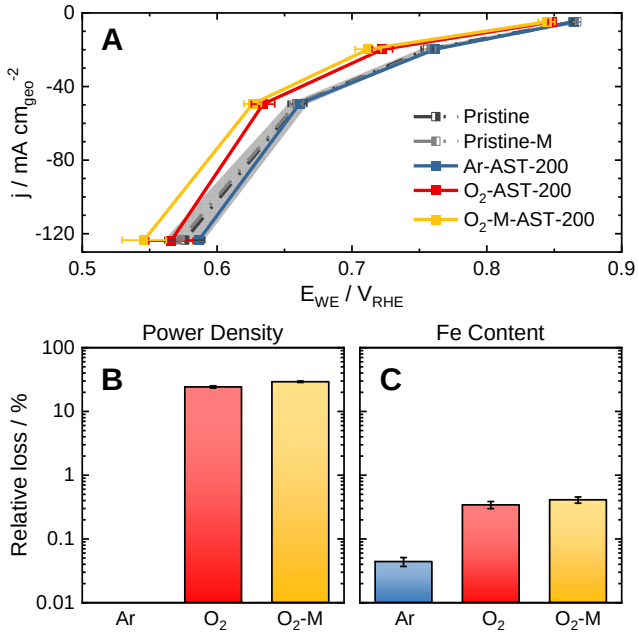

Figure 3. A: The polarization curves of the Fe-N-C GDEs in the following five conditions. (i) Before any AST, and without the thin AEM (Pristine, black), (ii) before any AST, and with the thin AEM (Pristine-M, grey), (iii) after the Ar-AST-200, and without the thin AEM (Ar-AST-200, blue), (iv) after the O_2-AST-200, and without the thin AEM (O_2-AST-200, red), and (v) after the O_2-AST-200, and with the thin AEM (O_2-M-AST-200, yellow). B & C: The relative losses of the power density at 0.65 V_{RHE} (B) and the Fe content (C) over the Ar-AST-200, O_2-AST-200, or O_2-M-AST-200 procedures. Note that the calculation of the loss of the Fe content is explained in section 1.3 of the SI.

After examining the effect of different relevant conditions on Fe dissolution, also the impact of catalyst dissolution on the catalyst activity should be compared (see Figure 3). First of all, when measuring ORR performance, no significant effect of the AEM on the initial activity (pristine) could be observed. Also, it is noteworthy that, if compared to the state-of-the-art AEMFCs literature values,[36] the ORR performance of the used electrocatalyst is inferior. We attribute this discrepancy to the relatively low concentration of alkaline electrolyte, i.e. 0.1 M NaOH, which is the highest concentration that the on-line ICP-MS can tolerate. Nevertheless, the activity test here is not designed for obtaining maximum performance but for comparing the effect of ASTs performed in the absence and presence of O_2 (ORR) on the same catalyst. Calculated from the polarization curves in Figure 3A, the relative loss of power density (PD) at 0.65 V_{RHE} is compared to the relative loss of Fe content in Figure 3B & 3C, first-hand indicating if the dissolved Fe species originally contribute to the activity or not. During the Ar-AST-200, only negligible performance deterioration occurred, although Fe dissolution was measurable (See Figure 3, blue). This can be interpreted as a small Fe dissolution during potential cycling in absence of O_2, but not specifically at the Fe active sites, or not at the most active sites. In contrast, regardless of whether there is an AEM coating or not, a similar and significant performance loss is detected after O_2-AST-200 (see Figure 3B). The relative losses of PD are above 20%. However, the relative losses of Fe during the O_2-AST-200 are only around 0.4 %, with or without an AEM coating (see Figure 3C). Similar trends of PD loss and Fe dissolution are also observed for Ar-AST-2k and O_2-AST-2k (see Figure S7B & S7C). Especially, although similar Fe contents were lost during O_2-AST-200 and Ar-AST-2k, the performance loss during O_2-AST-200 is more than 50 times higher than that during Ar-AST-2k. This implies that ORR could trigger Fe dissolution from species that contribute highly to the activity, or trigger modifications of the bulk or surface of the carbon matrix, in turn leading to decreased turnover frequency of the active sites, or both.

3.2 Impacts of ORR on the Dissolved Fe Species and on the Carbon Matrix

To identify which Fe species were dissolved during Ar-AST and O_2-AST, pristine and aged samples (no AST, Ar-AST-2k, and O_2-AST-2k) were post mortem characterized using several *ex situ* techniques, including X-ray absorption spectroscopy (XAS), scanning transmission electron microscopy (STEM), X-ray photoelectron spectroscopy (XPS), and Raman spectroscopy. First of all, the identified Fe species in this commercial Fe-N-C catalyst are FeN_xC_y, Fe_3C@N-C, and exposed Fe_3C nanoparticles. Fe_3C is suggested as the major Fe species by the Fourier transform (FT) of the extended X-ray absorption fine structure (EXAFS) spectra, characterized by a peak at about 2.08 Å, assigned to Fe-Fe backscattering in Fe_3C (see Figure S8). Also confirming the presence of Fe_3C with HRSTEM, lattice planes of the Fe-containing particles were captured and are shown in Figure S9A. In their respective diffractograms in Figure S9B, lattice spacings of 2.5 Å and 2.4 Å were identified, which correspond well to the planes (200) and (121) in the crystalline structure of Fe_3C. Furthermore, Figure S10 shows that many Fe_3C particles are encapsulated in graphite shells of thicknesses varying from about 2 nm to 12 nm (or even thicker). Moreover, these figures exhibit the interlayer spacing of the graphite shell being around 3.5 Å, similar to reported value for N-doped graphite shell around Fe_3C nanoparticles, usually denoted as Fe_3C@N-C.[37] As introduced before, these embedded Fe_3C particles are known to potentially boost the activity of the graphite shell or nearby FeN_xC_y active sites. Identifying FeN_xC_y, the XPS N-1s spectra (see

Figure 4A) show a notable peak at around 399.5 eV, which can be assigned either to specific N species or to N-Fe bonds.[30, 38] Furthermore, spectrum images (see EDX maps in Figure S11) indicate that besides Fe-containing nanoparticles, there is an additional Fe signal that is homogeneously distributed, even below the nanometric scale; Additionally, HAADF-HRSTEM reveals comparably bright spots at the atomic scale (see Figure S12). As this method exploits the mass-thickness contrast, these bright spots are heavier elements and thus can be assigned to atomically dispersed Fe-sites within the remarkably lighter carbon support. TEM analyses reveal the presence of FeN_xC_y sites in this material although its relative amount is suggested to be minor (< 5 %rel.) according to the EXAFS spectra. Note that the presence of graphite shells on the Fe_3C nanoparticles and the overall small amount of Fe in the catalyst explain the absence of Fe signal in XPS Fe-2p spectra (see Figure S13). In all cases in this study, it was not observed that the dissolved Fe species re-precipitate as Fe oxide, in contrast to a recent study performed in RDE conditions and for two other Fe-N-C catalysts, one rich in Fe_3C@N-C and the other rich in atomically dispersed FeN_xC_y sites.[12] The different tendencies of re-precipitation of leached Fe might be attributed to the different catalyst layer structures, ranges of current densities, and/or temperature. Although Fe dissolution is observed during Ar-AST-2k, the polarization curve, XPS N-1s and C-1s spectra barely change (see Figure S7, 4A & 4B). The unchanged XPS N-1s and C-1s spectra suggest the integrities of FeN_xC_y and Fe_3C@N-C, respectively. Because if FeN_xC_y site density had significantly decreased, the N-Fe signal in the N-1s spectrum (399.5 eV) would drop; if Fe dissolved from Fe_3C@N-C, the protecting graphite layer would already be compromised and thus the C-C signal in the C-1s spectrum would be lower. Therefore, Fe species which dissolve during Ar-AST-2k are likely the exposed Fe_3C nanoparticles, which do not contribute to the activity, explaining why the performance remained almost intact. During O_2-AST-2k, 3.4% of Fe and 34% of PD were lost (see Figure S7B & S7C), which is similar to the degradation of another Fe_3C@N-C species-rich Fe-N-C catalyst in an RDE setup, after 10k cycles of similar potential limits and step duration to those used in this work.[12] Herein, as the initial relative amount of FeN_xC_y sites is minor, the loss of FeN_xC_y sites could not be conclusively determined by either XANES or XPS. For example, in XPS N-1s spectra (see Figure 4A), the intensity at the N-Fe peak (399.5 eV) barely drops. Although there is a drop around 400.2 eV, this could not be exclusively assigned to a loss of FeN_xC_y or pyrrolic-N, of which the latter contributes to the peak at 401.1 eV and is noted as N3 in Figure 4A.[30] Nevertheless, even if the total Fe loss is comprised of some from FeN_xC_y sites, leading to decreasing SD, this specific loss would only partially explain the 34% loss of PD. On the contrary, Fe_3C particles with and without graphite shell both largely disappear during O_2-AST-2k, obviously observed with STEM (see Figure S14). Additionally, Figure 4B shows a drop of the C-C signal in the XPS C-1s spectrum and this confirms that the protecting graphite shell of Fe_3C@N-C could be compromised and thus new Fe_3C became exposed to the electrolyte, and started leaching. The loss of Fe_3C@N-C could lead in turn to a drop of the average TOF of FeN_xC_y sites of this catalyst, which could explain the 34% decrease in PD.

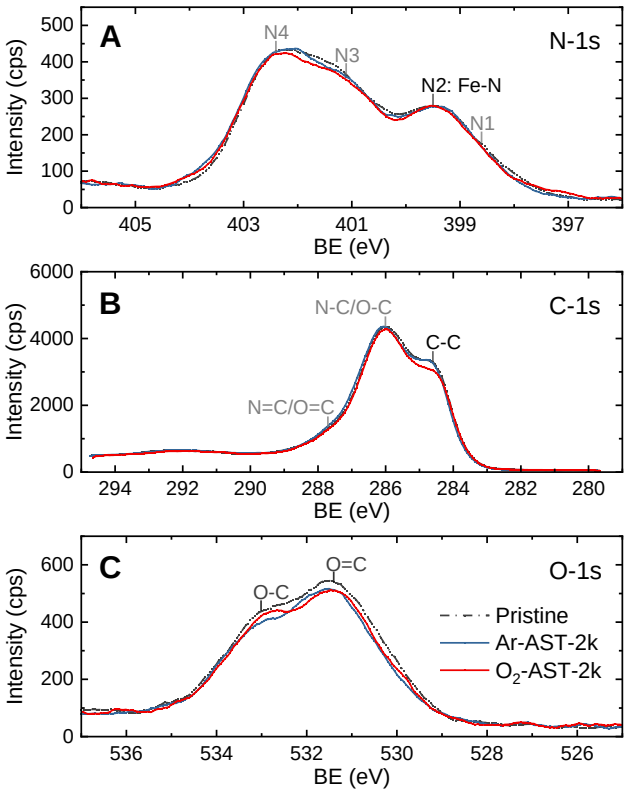

Figure 4. XPS spectra of the Fe-N-C GDEs that underwent (i) no AST (grey, desh-dotted line), (ii) Ar-AST-2k (blue, solid line), and (iii) O_2-AST-2k (red, solid line). A: XPS N-1s spectra, where N1, N2, N3, and N4 are assigned to pyridinic N, Fe-N, pyrrolic N, graphitic N, respectively.[30] B: XPS C-1s spectra, where the signal peaks are assigned to C species including those with C-C, C-O or –N, and C=O or =N bonds.[39] C: O-1s spectra, where the O species are assigned to O-C and O=C.[8]

As the decreased C-C signal in XPS C-1s spectrum of O_2-AST-2k (see Figure 4B) indicates a loss of graphite layers, the nature of the modification of the graphite structure during ORR in alkaline is further analyzed with Raman spectra and XPS O-1s spectra (see Figure S15 and 4C, respectively). Raman spectra show that the graphite crystallinity barely changed during O2-AST, or at least not as obviously as reported in acidic medium by Kumar *et al.*[14] Moreover, compared to the XPS O-1s spectrum of the pristine sample, those of the aged samples show decreased signals of both C-O and C=O species (oxygen functional groups). The opposite trend was observed by Choi *et al.*[16] and Bae *et al.*[8] upon the oxidation of graphite by ROS, suggesting a different nature of graphite modification in this study. Also, the decreased amounts of oxygen

functional groups suggest either the initially bonded O was reduced or that the O-bonded C was oxidized to gaseous CO or CO_2, the latter of which is known as the classic carbon corrosion. However, the rate of classic carbon corrosion is expected to increase with potential,[10, 40] while the rate of Fe dissolution increases with decreasing potential, in the studied potential range. Hence, the classic carbon corrosion is not considered dominating degradation mechanism under the studied conditions. To summarize the above analyses, while a negligible change in the graphite crystallinity and no further oxidation of the carbon matrix are suggested by the Raman and XPS O-1s spectra, respectively, the removal of a few graphite layers during ORR is indicated by XPS C-1s spectra.

The above unveils the impacts of ORR on the origins of dissolved Fe from Fe-N-C and on its graphite structure in alkaline media. With the presented data, some derivations on the degradation mechanism of Fe-N-C catalysts in alkaline media in realistic catalyst layers are made in the further course.

3.3 Fe Leaching Mechanism in Fe-N-C Catalysts in Alkaline Media

The degradation of Fe-N-C proceeds through diverse mechanisms in different electrochemical potential ranges or pH environments.[6, 10, 16] It has to be noted that the current work only allows derivations for the potential range between 1.0 and approximately 0.6 V_{RHE} in alkaline media. This, however, corresponds well to a usual potential range of AEMFCs under load.[41] Under the investigated conditions, the Fe dissolution is directly proportional to the applied charge for the Fe_3C@N-C species-rich Fe-N-C but also another benchmark Fe-N-C with dominant Fe species as FeN_xC_y (see Figure S16), the latter of which has been noted as $Fe_{0.5}$-NH_3 and well characterized previously.[42] In other words, for the two mainstream Fe-N-C catalysts for ORR in alkaline media, Fe dissolution can be largely correlated to charge transfer events. To start with the Fe_3C@N-C species-rich Fe-N-C, this correlation ties Fe dissolution from exposed Fe_3C particles to charge transfer events responding to electrochemical potential cycling during Ar-AST. Also, the same correlation associates Fe dissolution from Fe_3C@N-C with charge transfer events in ORR catalytic cycle. This association confirms that the dissolved Fe from Fe_3C@N-C were originally involved in ORR, at least indirectly. For example, Jiang *et al.*[18] reported that the step of adsorption of O_2 is more favored owing to additional electron provided to N atoms in FeN_xC_y sites by neighboring metallic Fe. In contrary, in $Fe_{0.5}$-NH_3 the dominant species FeN_xC_y is barely assisted by other Fe species to catalyze ORR. Meanwhile, the initial involvement of the dissolved Fe species in ORR is confirmed by the direct correlation between Fe dissolution and charge transfer events during ORR. Therefore, the dissolved Fe species during ORR in $Fe_{0.5}$-NH_3 should be mainly assigned to FeN_xC_y and thus Fe dissolution from FeN_xC_y sites can also be associated with the charge transfer events in ORR catalytic cycle. Consequently, both N-coordinated Fe at FeN_xC_y sites and the core-shell interface Fe of Fe_3C@N-C could be destabilized by one or more step(s) in the ORR catalytic cycle. To rationalize which step(s) dominates the Fe dissolution from Fe_3C@N-C and FeN_xC_y in alkaline media, the potential destabilizing steps, namely, the adsorption of O_2, the reduction of reaction intermediates, and the Fe redox transitions, are discussed below.

In the ORR where Fe_3C@N-C is involved, O_2 molecules could adsorb on activated graphite[19] and/or TOF-boosted FeN_xC_y site.[18] If O_2-adsorbing graphite is oxidized, then the initially protected Fe_3C@N-C could be exposed and lost. However, as discussed previously, XPS C-1s and O-1s spectra shown in Figure 4B & 4C suggest that the graphite was not further oxidized but removed. Thus, although the observed removal of graphite layers could be ORR-triggered, this may hardly be attributed to oxidation of graphite following the adsorption of O_2. On the other hand, according to density functional theory (DFT) calculations conducted by Aoyama *et al.*[43], the adsorption of O_2 molecules on Fe at FeN_xC_y sites can shift the Fe position from in-plane to out-of-plane. This could lead to a destabilization of the N-coordinated Fe cation and therefore to its dissolution. Although the DFT study was conducted for an acidic condition, we could not rule out the possibility that a similar destabilizing effect also occurs in alkaline media.

Secondly, the Fe active sites could also be destabilized by ORR intermediates, mainly HO_2^- (the dominating form of H_2O_2 in alkaline) or ROS.[34] The impact of H_2O_2 on the stability of Fe-N-C in acidic media has been systematically studied.[5, 14-16, 44] Choi *et al.*[16] and Bae *et al.*[8] performed H_2O_2-treatment on Fe-N-C in acidic or alkaline media, and found notable declines of the ORR activity after H_2O_2-treatments in acidic yet a negligible decrease after an H_2O_2–treatment in alkaline. This suggests that compared to H_2O_2 in acidic, HO_2^- is less harmful to Fe-N-C in alkaline environment, and thus its impact on the degradation process is potentially less pronounced. Actually in this work, as previously mentioned, the amounts of oxygen functional groups decrease during ORR in alkaline (see Figure 4C) as opposed to the effect of H_2O_2–treatment in acid.[8] Moreover, a great discrepancy is observed between the potential dependencies of the electric charge-normalized Fe dissolution detected in this work and the HO_2^- Faradaic efficiency reported for a similar catalyst in a previous work[31] (see Figure 5). Yet, it has to be considered that the Faradaic efficiency was determined in a rotating ring-disk electrode (RRDE) setup, where ORR is severely limited by the restricted mass transport of dissolved O_2 when the potential is below 0.8 V_{RHE}. This could lead to deviations when the RRDE result is compared to the dissolution data from this work, gathered from GDE half-cell measurements, where those mass transport limitations do not play a significant role.[25, 26, 27] Overall, the results point against a dominant impact of HO_2^- or ROS on the

stability of Fe-N-C in alkaline media and O_2 environment; however, with currently available data, it cannot be conclusively excluded either.

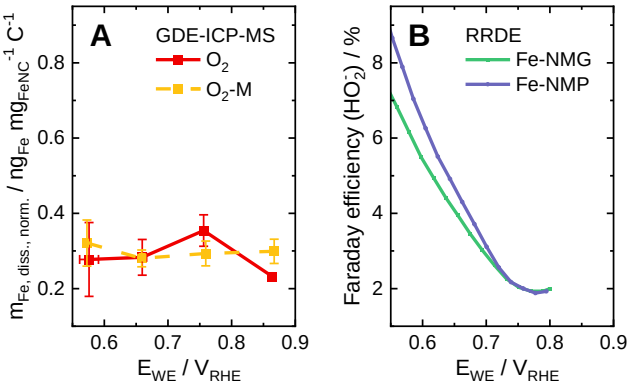

Figure 5. A: Correlation of the electric charge-normalized Fe dissolution with the applied potential during ORR in a GDE half-cell. The electric charge-normalized Fe dissolution is the integrated amount of Fe dissolution normalized to the applied charge and catalyst loading. B: Correlation of the Faradaic efficiency of HO_2^- with the applied potential during ORR in a rotating ring-disk electrode (RRDE) half-cell,[31] reprinted from *Journal of Power Sources*, 375, Hossen, M. M., *et al.*, Synthesis and characterization of high performing Fe-NC catalyst for oxygen reduction reaction (ORR) in Alkaline Exchange Membrane Fuel Cells, 214-221, Copyright (2018), with permission from Elsevier. Fe-NMG and Fe-NMP stand for Fe-N-C catalysts synthesized using different N-C precursors, Nicarbazin, Methylimidazole and Glucoril for Fe-NMG, and Nicarbazin, Methylimidazole and Pipemedic Acid for Fe-NMP.[31]

Thirdly, in a previous online dissolution study, the onsets of transition-metal dissolution in PGM-free catalysts (manganese oxide MnO_x) could be correlated to the corresponding redox transition potentials.[23] It was proposed that the reconstruction of the surface MnO_x coordination during redox transitions could lead to the so-called transient-dissolution. Although the structures of MnO_x and the Fe species in Fe-N-C are different and this demetallation mechanism has not been identified responsible for degradations of Fe-N-C catalysts yet, a similar concept could still be applied. Namely, the ORR-triggered redox transition of the Fe on the core-shell interface of Fe_3C@N-C leads to the coordination reconstruction of the core-shell interface of Fe_3C@N-C. Consequently, the continuous reconstruction of the core-shell interface may create defects on the interface, potentially detaching the graphite shell from the Fe_3C core, and thereby exposing the Fe_3C core to the electrolyte. Additionally, during ORR the Fe^{3+}/Fe^{2+} redox transition (see Equation (1) and (2) below) at FeN_xC_y sites and its corresponding changes of coordination could result in transient instability of the coordinated Fe, and thus potentially drive its dissolution.

$$N_4Fe^{2+}\cdots O_aH_b \longrightarrow N_4Fe^{3+}\cdots O_aH_b{}^- \quad (1)$$

$$N_4Fe^{3+}\cdots O_cH_d + e^- \longrightarrow N_4Fe^{2+}\cdots O_cH_d \quad (2)$$

From the Fe dissolution data during ORR, any destabilizing step during the ORR catalytic cycle could be suspected to be responsible for the Fe demetallation in Fe-N-C. However, more insights may be gained from the surprisingly similar values of the electric charge-normalized Fe dissolution during the O_2-AST and Ar-AST (see Figure 2B & S16). This implies that the key destabilizing factor to the Fe dissolution in Fe-N-C in alkaline media could be one that is related to charge transfer events and that also occurs in both O_2-AST and Ar-AST. Among the three above mentioned destabilizing factors during ORR, only Fe redox transitions also take place during the Ar-AST. Indeed, charge-discharge processes may result in the Fe dissolution from exposed Fe_3C particles.[11, 45] Moreover, the correlation between Fe^{3+}/Fe^{2+} redox transition and the stability of Fe at FeN_xC_y sites in the absence of O_2 could be supported by the findings revealed by Li *et al.*[21] They reported that the Fe active sites that undergo reversible Fe^{3+}/Fe^{2+} redox transitions due to potential switches between 0.2 and 0.8 V_{RHE} (FeN_4C_{12}) are less stable than those where the charge of Fe ions (2+) is constant and independent of the potential switches (FeN_4C_{10}). This supports the idea that the N-coordinated Fe could be less stable during its redox transitions even in the absence of O_2.

Hence, we propose that the Fe dissolution from FeN_xC_y sites in alkaline media can be attributed to the instability of the coordinated Fe during the Fe^{3+}/Fe^{2+} redox transition. As for Fe_3C@N-C in alkaline media, the ORR-triggered Fe redox transition destabilizes the core-shell interface and potentially detaches the graphite shell from the Fe_3C core, at least locally. If the exposed Fe on the partially covered Fe_3C core is still involved in the ORR occurring at its neighboring active sites, the ORR-triggered Fe redox transition would continue destabilizing this exposed Fe and thus cause its dissolution. Or if the exposed Fe is not involved in any ORR, it would be destabilized by its redox transition triggered by potential cycling as in the Ar case. This hypothesis can also explain the different amounts and the varied ORR-activity contributions of the dissolved Fe species in the absence and presence of ORR: On the one hand, the Fe redox transition in an Ar-saturated environment would only be triggered by the change of electrochemical potential, occurring only twice in each AST cycle. Also, the transitioned Fe species do not necessarily have high activity. On the other hand, in the presence of O_2, the Fe involved in ORR continuously undergo redox transitions in the first half of each AST cycle. Moreover, the more active the FeN_xC_y sites are, the more frequent the involved Fe species undergo the redox transitions. Therefore, during the O_2-AST, the Fe dissolution from the FeN_xC_y or Fe_3C@N-C that contribute highly to the ORR activity is more significant than that during the Ar-AST.

4. Conclusions and Outlook

In the present work, Fe demetallation of Fe-N-C catalyst layers in alkaline media is studied at realistic conditions, such as O_2 environment, elevated current densities, and a thin AEM on the catalyst layer. We show that Fe dissolution is significantly enhanced in O_2 environment compared to Ar. Additionally, Fe dissolution is shown to be directly proportional to the applied charge. We identified that in the Fe_3C@N-C species-rich Fe-N-C, Fe is dissolved from exposed Fe_3C nanoparticles responding to potential cycling, while the Fe dissolution from Fe_3C@N-C that are involved in ORR follows ORR-triggered removal of the protective graphite shell. Moreover, we discovered for both Fe_3C@N-C species-rich and FeN_xC_y species-rich Fe-N-C catalysts, a strong correlation between Fe redox transitions and the Fe dissolution in the presence and absence of ORR in the studied potential range, 1.0 – 0.57 V_{RHE}. This leads to our hypothesis that the instability of Fe during the redox transitions could be predominantly responsible for the Fe demetallation in Fe-N-C catalysts in alkaline media. This hypothesis could help rationalizing the different scales and origins of the Fe dissolution in the presence and absence of ORR. For future work, Fe-N-C catalysts with solely Fe_3C@N-C species, solely FeN_xC_y species, and with both, should be evaluated with GDE-ICP-MS in different potential regions. In addition to the applied *ex situ* techniques in this work, the Fe dissolution data should be accompanied with post mortem Mössbauer spectroscopy (necessitating ^{57}Fe enriched samples),[13, 21] in order to rationalize the structure-stability relationship of Fe-N-C catalysts in more detail. Based on that, strategies for improving the stability of Fe-N-C catalysts dedicated for AEMFCs need to be developed, since the dominant degradation mechanism of Fe-N-C catalysts might be different in alkaline compared to acidic environment.

ASSOCIATED CONTENT

The Supporting Information is available free of charge via the Internet at http://pubs.acs.org.

A scheme of GDE-ICP-MS setup; experimental details; details of data analysis; SEM images for thickness analysis; supporting dissolution and electrochemical data; FT-EXAFS spectra; STEM micrographs; and Raman spectra.

AUTHOR INFORMATION

Corresponding Author

*Yu-Ping Ku - Forschungszentrum Jülich GmbH, Helmholtz-Institute Erlangen-Nürnberg for Renewable Energy (IEK-11), Cauerstraße 1, 91058 Erlangen, Germany; Department of Chemical and Biological Engineering, Friedrich-Alexander University Erlangen-Nürnberg, Cauerstraße 1, 91058 Erlangen, Germany; Email: y.ku@fz-juelich.de

*Frédéric Jaouen - Institut Charles Gerhardt Montpellier, Univ. Montpellier, CNRS, ENSCM, 1919 route de Mende, F-34293 Montpellier, France; Email: frederic.jaouen@umontpellier.fr

*Serhiy Cherevko - Forschungszentrum Jülich GmbH, Helmholtz-Institute Erlangen-Nürnberg for Renewable Energy (IEK-11), Cauerstraße 1, 91058 Erlangen, Germany; Email: s.cherevko@fz-juelich.de

Author Contributions

All authors have given approval to the final version of the manuscript.

ACKNOWLEDGMENT

YPK acknowledges Jonas Möller for software development for data analysis, Matej Zlatar, Christian Göllner, Dr. Attila Kormanyos, and Dr. Daniel Escalera for technical support during ICP-MS measurements, Yi-Jia Tsai for visualizing the graphic abstract, Funda Arslan and Guangxin Liu for sharing crucial electrochemical equipment. KE acknowledges Heinrich Böll Foundation for financial support. The project CREATE leading to this application has received funding from the European Union's Horizon 2020 research and innovation programme under grant agreement No. 721065.

REFERENCES

(1) Bockris, J. O. M. A Hydrogen Economy. *Science* **1972**, *176* (4041), 1323-1323. DOI: 10.1126/science.176.4041.1323.

(2) Pivovar, B. Catalysts for fuel cell transportation and hydrogen related uses. *Nat. Catal.* **2019**, *2* (7), 562-565. DOI: 10.1038/s41929-019-0320-9.

(3) Du, L.; Prabhakaran, V.; Xie, X.; Park, S.; Wang, Y.; Shao, Y. Low-PGM and PGM-Free Catalysts for Proton Exchange Membrane Fuel Cells: Stability Challenges and Material Solutions. *Adv. Mater.* **2021**, *33* (6), 1908232. DOI: 10.1002/adma.201908232. Wang, X. X.; Swihart, M. T.; Wu, G. Achievements, challenges and perspectives on cathode catalysts in proton exchange membrane fuel cells for transportation. *Nat. Catal.* **2019**, *2* (7), 578-589. DOI: 10.1038/s41929-019-0304-9. Thompson, S. T.; Papageorgopoulos, D. Platinum group metal-free catalysts boost cost competitiveness of fuel cell vehicles. *Nat. Catal.* **2019**, *2* (7), 558-561. DOI: 10.1038/s41929-019-0291-x.

(4) Martinez, U.; Komini Babu, S.; Holby, E. F.; Chung, H. T.; Yin, X.; Zelenay, P. Progress in the development of Fe-based PGM-free electrocatalysts for the oxygen reduction reaction. *Adv. Mater.* **2019**, *31* (31), 1806545. DOI: 10.1002/adma.201806545.

(5) Speck, F. D.; Kim, J. H.; Bae, G.; Joo, S. H.; Mayrhofer, K. J. J.; Choi, C. H.; Cherevko, S. Single-Atom Catalysts: A Perspective toward Application in Electrochemical Energy Conversion. *J. Am. Chem. Soc. Au* **2021**, *1* (8), 1086-1100. DOI: 10.1021/jacsau.1c00121.

(6) Santori, P. G.; Speck, F. D.; Li, J.; Zitolo, A.; Jia, Q.; Mukerjee, S.; Cherevko, S.; Jaouen, F. Effect of Pyrolysis Atmosphere and Electrolyte pH on the Oxygen Reduction Activity, Stability and Spectroscopic

Signature of FeN_x Moieties in Fe-N-C Catalysts. *J. Electrochem. Soc.* **2019**, *166* (7), F3311. DOI: 10.1149/2.0371907jes.
(7) Holby, E. F.; Wang, G.; Zelenay, P. Acid Stability and Demetalation of PGM-Free ORR Electrocatalyst Structures from Density Functional Theory: A Model for "Single-Atom Catalyst" Dissolution. *ACS Catal.* **2020**, *10*, 14527-14539. DOI: 10.1021/acscatal.0c02856.
(8) Bae, G.; Chung, M. W.; Ji, S. G.; Jaouen, F.; Choi, C. H. PH Effect on the H_2O_2-Induced Deactivation of Fe-N-C Catalysts. *ACS Catal.* **2020**, *10* (15), 8485-8495. DOI: 10.1021/acscatal.0c00948.
(9) Serov, A.; Zenyuk, I. V.; Arges, C. G.; Chatenet, M. Hot topics in alkaline exchange membrane fuel cells. *J. Power Sources* **2018**, *375*, 149-157. DOI: 10.1016/j.jpowsour.2017.09.068. Firouzjaie, H. A.; Mustain, W. E. Catalytic Advantages, Challenges, and Priorities in Alkaline Membrane Fuel Cells. **2019**, *10* (1), 225-234. DOI: 10.1021/acscatal.9b03892. Dekel, D. R. Review of cell performance in anion exchange membrane fuel cells. *J. Power Sources* **2018**, *375*, 158-169. DOI: 10.1016/j.jpowsour.2017.07.117. Varcoe, J. R.; Atanassov, P.; Dekel, D. R.; Herring, A. M.; Hickner, M. A.; Kohl, P. A.; Kucernak, A. R.; Mustain, W. E.; Nijmeijer, K.; Scott, K.; et al. Anion-exchange membranes in electrochemical energy systems. *Energy Environ. Sci.* **2014**, *7* (10), 3135-3191. DOI: 10.1039/C4EE01303D.
(10) Choi, C. H.; Baldizzone, C.; Grote, J.-P.; Schuppert, A. K.; Jaouen, F.; Mayrhofer, K. J. J. Stability of Fe-N-C Catalysts in Acidic Medium Studied by Operando Spectroscopy. *Angew. Chem. Int. Ed.* **2015**, *54* (43), 12753-12757. DOI: 10.1002/anie.201504903.
(11) Choi, C. H.; Baldizzone, C.; Polymeros, G.; Pizzutilo, E.; Kasian, O.; Schuppert, A. K.; Ranjbar Sahraie, N.; Sougrati, M.-T.; Mayrhofer, K. J. J.; Jaouen, F. Minimizing Operando Demetallation of Fe-N-C Electrocatalysts in Acidic Medium. *ACS Catal.* **2016**, *6* (5), 3136-3146. DOI: 10.1021/acscatal.6b00643.
(12) Sgarbi, R.; Kumar, K.; Saveleva, V. A.; Dubau, L.; Chattot, R.; Martin, V.; Mermoux, M.; Bordet, P.; Glatzel, P.; Ticianelli, E. A.; et al. Electrochemical Transformation of Fe-N-C catalysts into Iron Oxides in Alkaline Medium and Its Impact on the Oxygen Reduction Reaction Activity. *Applied Catalysis B: Environmental* **2022**, *311*, 121366. DOI: 10.1016/j.apcatb.2022.121366.
(13) Chenitz, R.; Kramm, U. I.; Lefèvre, M.; Glibin, V.; Zhang, G.; Sun, S.; Dodelet, J.-P. A specific demetalation of $Fe–N_4$ catalytic sites in the micropores of NC_Ar + NH_3 is at the origin of the initial activity loss of the highly active Fe/N/C catalyst used for the reduction of oxygen in PEM fuel cells. *Energy Environ. Sci.* **2018**, *11* (2), 365-382. DOI: 10.1039/C7EE02302B.
(14) Kumar, K.; Dubau, L.; Mermoux, M.; Li, J.; Zitolo, A.; Nelayah, J.; Jaouen, F.; Maillard, F. On the Influence of Oxygen on the Degradation of Fe-N-C Catalysts. *Angew. Chem.* **2020**, *132* (8), 3261-3269. DOI: 10.1002/anie.201912451.
(15) Lefèvre, M.; Dodelet, J.-P. Fe-based catalysts for the reduction of oxygen in polymer electrolyte membrane fuel cell conditions: determination of the amount of peroxide released during electroreduction and its influence on the stability of the catalysts. *Electrochim. Acta* **2003**, *48* (19), 2749-2760. DOI: 10.1016/S0013-4686(03)00393-1.
(16) Choi, C. H.; Lim, H.-K.; Chung, M. W.; Chon, G.; Ranjbar Sahraie, N.; Altin, A.; Sougrati, M.-T.; Stievano, L.; Oh, H. S.; Park, E. S.; et al. The Achilles' heel of iron-based catalysts during oxygen reduction in an acidic medium. *Energy Environ. Sci.* **2018**, *11* (11), 3176-3182. DOI: 10.1039/C8EE01855C.
(17) Kumar, K.; Asset, T.; Li, X.; Liu, Y.; Yan, X.; Chen, Y.; Mermoux, M.; Pan, X.; Atanassov, P.; Maillard, F.; et al. Fe–N–C Electrocatalysts' Durability: Effects of Single Atoms' Mobility and Clustering. *ACS Catal.* **2020**, *11* (2), 484-494. DOI: 10.1021/acscatal.0c04625.
(18) Jiang, W.-J.; Gu, L.; Li, L.; Zhang, Y.; Zhang, X.; Zhang, L.-J.; Wang, J.-Q.; Hu, J.-S.; Wei, Z.; Wan, L.-J. Understanding the High Activity of Fe–N–C Electrocatalysts in Oxygen Reduction: Fe/Fe_3C Nanoparticles Boost the Activity of $Fe–N_x$. *J. Am. Chem. Soc.* **2016**, *138* (10), 3570-3578. DOI: 10.1021/jacs.6b00757.
(19) Deng, D.; Yu, L.; Chen, X.; Wang, G.; Jin, L.; Pan, X.; Deng, J.; Sun, G.; Bao, X. Iron Encapsulated within Pod-like Carbon Nanotubes for Oxygen Reduction Reaction. *Angew. Chem.* **2013**, *125* (1), 389-393.
(20) Sgarbi, R.; Kumar, K.; Jaouen, F.; Zitolo, A.; Ticianelli, E. A.; Maillard, F. Oxygen reduction reaction mechanism and kinetics on M-NxCy and M@N-C active sites present in model M-N-C catalysts under alkaline and acidic conditions. *Journal of Solid State Electrochemistry* **2021**, *25* (1), 45-56. DOI: 10.1007/s10008-019-04436-w.
(21) Li, J.; Sougrati, M. T.; Zitolo, A.; Ablett, J. M.; Oğuz, I. C.; Mineva, T.; Matanovic, I.; Atanassov, P.; Huang, Y.; Zenyuk, I.; et al. Identification of durable and non-durable FeN_x sites in Fe–N–C materials for proton exchange membrane fuel cells. *Nat. Catal.* **2021**, *4* (1), 10-19. DOI: 10.1038/s41929-020-00545-2.
(22) Ehelebe, K.; Escalera-López, D.; Cherevko, S. Limitations of aqueous model systems in the stability assessment of electrocatalysts for oxygen reactions in fuel cell and electrolysers. *Curr. Opin. Electrochem.* **2021**, *29*, 100832. DOI: 10.1016/j.coelec.2021.100832.
(23) Speck, F. D.; Santori, P. G.; Jaouen, F.; Cherevko, S. Mechanisms of Manganese Oxide Electrocatalysts Degradation during Oxygen Reduction and Oxygen

Evolution Reactions. *J. Phys. Chem. C* **2019**, *123* (41), 25267-25277. DOI: 10.1021/acs.jpcc.9b07751.
(24) Osmieri, L.; Cullen, D. A.; Chung, H. T.; Ahluwalia, R. K.; Neyerlin, K. C. Durability evaluation of a Fe–N–C catalyst in polymer electrolyte fuel cell environment via accelerated stress tests. *Nano Energy* **2020**, *78*, 105209. DOI: 10.1016/j.nanoen.2020.105209.
(25) Lin, X.; Zalitis, C. M.; Sharman, J.; Kucernak, A. Electrocatalyst Performance at the Gas/Electrolyte Interface under High-Mass-Transport Conditions: Optimization of the "Floating Electrode" Method. *ACS Appl. Mater. Interfaces* **2020**, *12* (42), 47467-47481. DOI: 10.1021/acsami.0c12718. Inaba, M.; Jensen, A. W.; Sievers, G. W.; Escudero-Escribano, M.; Zana, A.; Arenz, M. Benchmarking high surface area electrocatalysts in a gas diffusion electrode: measurement of oxygen reduction activities under realistic conditions. *Energy Environ. Sci.* **2018**, *11* (4), 988-994. DOI: 10.1039/C8EE00019K.
(26) Pinaud, B. A.; Bonakdarpour, A.; Daniel, L.; Sharman, J.; Wilkinson, D. P. Key considerations for high current fuel cell catalyst testing in an electrochemical half-cell. *J. Electrochem. Soc.* **2017**, *164* (4), F321. DOI: 10.1149/2.0891704jes.
(27) Ehelebe, K.; Seeberger, D.; Paul, M. T. Y.; Thiele, S.; Mayrhofer, K. J. J.; Cherevko, S. Evaluating Electrocatalysts at Relevant Currents in a Half-Cell: The Impact of Pt Loading on Oxygen Reduction Reaction. *J. Electrochem. Soc.* **2019**, *166* (16), F1259. DOI: 10.1149/2.0911915jes.
(28) Ehelebe, K.; Ashraf, T.; Hager, S.; Seeberger, D.; Thiele, S.; Cherevko, S. Fuel cell catalyst layer evaluation using a gas diffusion electrode half-cell: Oxygen reduction reaction on Fe-N-C in alkaline media. *Electrochem. commun.* **2020**, *116*, 106761. DOI: 10.1016/j.elecom.2020.106761.
(29) Ehelebe, K.; Knöppel, J.; Bierling, M.; Mayerhöfer, B.; Böhm, T.; Kulyk, N.; Thiele, S.; Mayrhofer, K. J. J.; Cherevko, S. Platinum Dissolution in Realistic Fuel Cell Catalyst Layers. *Angew. Chem. Int. Ed.* **2021**, *60* (16), 8882-8888. DOI: 10.1002/ange.202014711.
(30) Primbs, M.; Sun, Y.; Roy, A.; Malko, D.; Mehmood, A.; Sougrati, M.-T.; Blanchard, P.-Y.; Granozzi, G.; Kosmala, T.; Daniel, G.; et al. Establishing reactivity descriptors for platinum group metal (PGM)-free Fe–N–C catalysts for PEM fuel cells. *Energy Environ. Sci.* **2020**, *13* (8), 2480-2500. DOI: 10.1039/D0EE01013H.
(31) Hossen, M. M.; Artyushkova, K.; Atanassov, P.; Serov, A. Synthesis and characterization of high performing Fe-N-C catalyst for oxygen reduction reaction (ORR) in Alkaline Exchange Membrane Fuel Cells. *J. Power Sources* **2018**, *375*, 214-221. DOI: 10.1016/j.jpowsour.2017.08.036.
(32) Geiger, S.; Kasian, O.; Ledendecker, M.; Pizzutilo, E.; Mingers, A. M.; Fu, W. T.; Diaz-Morales, O.; Li, Z.; Oellers, T.; Fruchter, L.; et al. The stability number as a metric for electrocatalyst stability benchmarking. *Nat. Catal.* **2018**, *1* (7), 508-515. DOI: 10.1038/s41929-018-0085-6.
(33) Zhang, G.; Chenitz, R.; Lefèvre, M.; Sun, S.; Dodelet, J.-P. Is iron involved in the lack of stability of Fe/N/C electrocatalysts used to reduce oxygen at the cathode of PEM fuel cells? *Nano Energy* **2016**, *29*, 111-125. DOI: 10.1016/j.nanoen.2016.02.038.
(34) Ramaswamy, N.; Tylus, U.; Jia, Q.; Mukerjee, S. Activity Descriptor Identification for Oxygen Reduction on Nonprecious Electrocatalysts: Linking Surface Science to Coordination Chemistry. *J. Am. Chem. Soc.* **2013**, *135* (41), 15443-15449. DOI: 10.1021/ja405149m.
(35) Ramaswamy, N.; Mukerjee, S. Alkaline Anion-Exchange Membrane Fuel Cells: Challenges in Electrocatalysis and Interfacial Charge Transfer. *Chem. Rev.* **2019**, *119* (23), 11945-11979. DOI: 10.1021/acs.chemrev.9b00157.
(36) Adabi, H.; Shakouri, A.; Ul Hassan, N.; Varcoe, J. R.; Zulevi, B.; Serov, A.; Regalbuto, J. R.; Mustain, W. E. High-performing commercial Fe–N–C cathode electrocatalyst for anion-exchange membrane fuel cells. *Nature Energy* **2021**, *6* (8), 834-843. DOI: 10.1038/s41560-021-00878-7.
(37) Kumar, K.; Gairola, P.; Lions, M.; Ranjbar-Sahraie, N.; Mermoux, M.; Dubau, L.; Zitolo, A.; Jaouen, F.; Maillard, F. Physical and Chemical Considerations for Improving Catalytic Activity and Stability of Non-Precious-Metal Oxygen Reduction Reaction Catalysts. *ACS Catal.* **2018**, *8* (12), 11264-11276. DOI: 10.1021/acscatal.8b02934.
(38) Matanovic, I.; Artyushkova, K.; Atanassov, P. Understanding PGM-free catalysts by linking density functional theory calculations and structural analysis: Perspectives and challenges. *Curr. Opin. Electrochem.* **2018**, *9*, 137-144. DOI: 10.1016/j.coelec.2018.03.009.
(39) Gupta, S.; Qiao, L.; Zhao, S.; Xu, H.; Lin, Y.; Devaguptapu, S. V.; Wang, X.; Swihart, M. T.; Wu, G. Highly Active and Stable Graphene Tubes Decorated with FeCoNi Alloy Nanoparticles via a Template-Free Graphitization for Bifunctional Oxygen Reduction and Evolution. *Advanced Energy Materials* **2016**, *6* (22), 1601198. DOI: 10.1002/aenm.201601198. Zhang, L.; Wang, X.; Wang, R.; Hong, M. Structural Evolution from Metal–Organic Framework to Hybrids of Nitrogen-Doped Porous Carbon and Carbon Nanotubes for Enhanced Oxygen Reduction Activity. *Chemistry of Materials* **2015**, *27* (22), 7610-7618. DOI: 10.1021/acs.chemmater.5b02708.
(40) Kumar, K.; Gairola, P.; Lions, M.; Ranjbar Sahraie, N.; Mermoux, M.; Dubau, L.; Zitolo, A.; Jaouen, F.; Maillard, F. Physical and Chemical Considerations for Improving Catalytic Activity and Stability of Non-Precious-Metal Oxygen Reduction Reaction Catalysts.

ACS Catal. **2018**, *8* (12), 11264-11276. DOI: 10.1021/acscatal.8b02934.
(41) Mustain, W. E.; Chatenet, M.; Page, M.; Kim, Y. S. Durability challenges of anion exchange membrane fuel cells. *Energy Environ. Sci.* **2020**, *13* (9), 2805-2838. DOI: 10.1039/D0EE01133A.
(42) Zitolo, A.; Goellner, V.; Armel, V.; Sougrati, M.-T.; Mineva, T.; Stievano, L.; Fonda, E.; Jaouen, F. Identification of catalytic sites for oxygen reduction in iron- and nitrogen-doped graphene materials. *Nature Materials* **2015**, *14* (9), 937-942. DOI: 10.1038/nmat4367.
(43) Aoyama, S.; Kaiwa, J.; Chantngarm, P.; Tanibayashi, S.; Saito, H.; Hasegawa, M.; Nishidate, K. Oxygen reduction reaction of FeN_4 center embedded in graphene and carbon nanotube: Density functional calculations. *AIP Adv.* **2018**, *8* (11), 115113. DOI: 10.1063/1.5053151.
(44) Choi, C. H.; Choi, W. S.; Kasian, O.; Mechler, A. K.; Sougrati, M. T.; Brüller, S.; Strickland, K.; Jia, Q.; Mukerjee, S.; Mayrhofer, K. J. J.; et al. Unraveling the Nature of Sites Active toward Hydrogen Peroxide Reduction in Fe-N-C Catalysts. *Angew. Chem. Int. Ed.* **2017**, *56* (30), 8809-8812. DOI: 10.1002/anie.201704356.
(45) Ujimine, K.; Tsutsumi, A. Electrochemical characteristics of iron carbide as an active material in alkaline batteries. *J. Power Sources* **2006**, *160* (2), 1431-1435. DOI: 10.1016/j.jpowsour.2006.03.002.

Table of Contents (TOC)